Influence of quench rate on multi-stage ageing of AA6014 alloy

Zi Yang[1,*], *Xiaohe* Jiang [1], *Xingpu* Zhang[1], *Meng* Liu[1], *Zeqin* Liang[2], *David* Leyvraz[2]and *John* Banhart[1]

[1]Helmholtz-Centre Berlin for Materials and Energy, Hahn-Meitner-Platz 1, 14109 Berlin, Germany
[2]Novelis R&T Centre, Sierre, Route des Laminoirs 15, 3960 Sierre, Switzerland

Abstract. The influence of quench rate after solution heat treatment on the microstructure in the as-quenched state and subsequent ageing kinetics of alloy AA6014 was investigated by means of transmission electron microscopy, positron annihilation lifetime spectroscopy and hardness measurements. Various ageing temperatures and stages were taken into consideration. Consistent with previous studies, we found that solute and vacancy supersaturation decrease during slow quenching due to precipitation and annihilation, respectively. Additionally, we observed cluster formation during cooling below 200 °C. As for the influence on ageing behaviour we observe different behaviour for high and low ageing temperature: Artificial ageing is more affected than pre-ageing and natural secondary ageing. The detrimental effect of natural ageing on paint-bake hardening also depends on the quench rate. Possible interpretations are associated with cluster formation during natural ageing and also during quenching. The influence of pre-ageing at different temperatures on subsequent ageing kinetics is similar for slower industrial-type quenching and for fast quenching, thus allowing to apply the findings from idealised quenching conditions to situations closer to real application.

1 Introduction

Precipitation hardening is the main method for strengthening the Al-Mg-Si alloys (6000 series). As the first step after solution heat treatment (SHT), quenching plays a crucial role as it ensures the high level of dissolved solute atoms and trapped excess vacancies necessary for precipitate formation during the ensuing natural or artificial ageing (NA/AA). In laboratory conditions, quenching is most often carried out in water, which is convenient, efficient, and reproducible. However, quenching in industrial production can be much slower due to much larger sample volumes and other factors. Investigating the quenching procedure is therefore a task of great practical relevance.

Studies of quench sensitivity have shown that slower quenching can limit the maximum hardenability of the Al-Mg-Si alloys during direct AA [1-3]. However, a peculiarity of this type of alloy appears when applying multi-stage ageing treatments, i.e. hardening during AA is dependent also on previous ageing treatments. A classic example is that for alloys containing more than 1 at.% solute atoms, NA at 'room temperature' introduces a detrimental effect on subsequent AA, while pre-ageing (PA) at intermediate temperatures, e.g. 100 °C, does not [4-6]. Moreover, PA also suppresses hardening during subsequent natural secondary ageing (NSA) and also enhances the final paint-bake (PB) response [7, 8], the effect of which is determined by the PA temperature [9]. However, whether the multi-stage ageing behaviour will be influenced by the quench conditions has been studied only recently, when the combined effect of quench rate and NA on AA was investigated on two different alloys [10, 11], but the mechanisms still remain elusive. Hence, in this study we aim to elucidate the influence of quench rate on the microstructure as well as on the following single-, two-, and multi-stage ageing treatments.

2 Experimental

Alloy AA6014 (0.65% Mg, 0.60% Si, 0.18% Fe, 0.08% Mn, 0.12% Cu, all in wt.%) was provided by Novelis Switzerland. Square samples with a geometry of ~10×10×1 mm^3 were prepared. SHT was conducted at 540 °C for 1 h in an air circulation furnace. Two principal types of quenches were performed. In the first type (T1), samples were quenched in one step either in ice-water (IWQ), in the air flow of a ventilator (ventilator cooling, or VC), or in resting air (air cooling, or AC) to the ambient temperature. In the second two-step type (T2), the process of VC or AC was interrupted at a given target temperature by applying a subsequent fast quench in ice water. 'VC_*x*' or 'AC_*x*' are used to label the samples after T2 quench, where *x* stands for a target temperature, which was controlled within ±15 °C for VC and ±5 °C for AC. Fig. 1 shows the temperature evolution during quenching, which is measured by a thermocouple inserted in the hole on the side of a dummy sample. Quench rates from 533 °C to 250 °C are in average >980 K/s for IWQ, ~27 K/s for VC, and ~5 K/s for AC, respectively. The VC quenching is close to industrial cooling conditions. Subsequent ageing was performed in an oil bath at (180.0 ± 0.2) °C for AA, and (100.0 ± 0.2) °C for PA or in a Peltier-cooled incubator at 20 ± 0.1 °C (NA and NSA). AA for 30 min at 180 °C

* Corresponding author: zi.yang@helmholtz-berlin.de

is used in this study to imitate the industrial paint-baking (PB). The time required for transferring samples from the quenching device to the oil bath for ageing is ~0.5 min. Single-stage (AA) and some multi-stage ageing treatments (NA+PB) were performed on all three T1-type cooled samples, while multi-stage ageing involving PA (PA+PB, PA+NSA, and PA+NSA+PB) were only performed on IWQ and VC samples. In the following, the abbreviation 'PA *x*/*y*' stands for PA at *x* °C for *y* min.

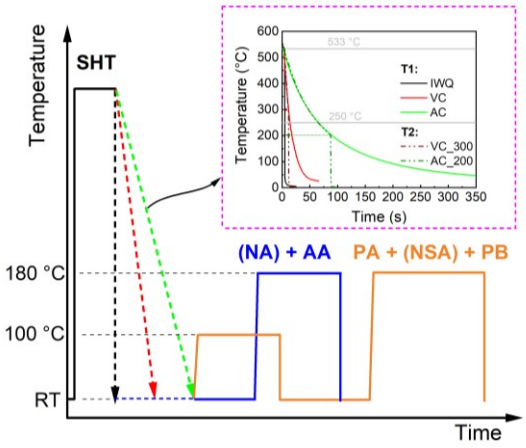

Fig. 1. Schematic illustration of the heat treatments applied to the alloy. Inset shows the measured temperature profile during various quenching conditions.

Brinell hardness was measured on a hardness tester (Qness, model 60M) using a load of 10 kgf for 10 s and a tungsten carbide indenter of 1 mm diameter. Eight indentations were performed on each sample for calculating the average, which ensures a standard error of <1 HBW for >98% of the measurements. TEM characterisation was performed on a Philips CM30 unit operated at 300 kV and equipped with an energy dispersive X-ray (EDX) spectrometer. The electron beam was aligned along a 〈100〉 direction of the Al matrix. TEM foils were prepared by mechanical thinning and then twin-jet electro-polishing in an electrolyte mixture of 75% methanol and 25% nitric acid. Positron annihilation lifetime spectroscopy (PALS) was performed after various quenches to probe the microstructure evolution during quenching. Such technique measures the lifetimes of positrons after production from the source and before annihilating with electrons in the material. Therefore, this technique possesses a unique sensitivity to the local electron density change, such as caused by solute clusters and, in particular, vacancies, because there very low electron density presents and thus markedly higher positron lifetimes are resulted. In this study, positrons were produced by a $^{22}NaCO_3$ source enveloped in kapton foil, which was sandwiched by two square samples during measurement. The resolution (FWHM) of the spectrometer was ~200 ps, and software LT9 was used to determine the one-component lifetimes, which represents an weighted average of positron lifetimes in all microstructural features.

3 Results

3.1 Transmission electron microscopy

Microstructure after all three T1-type quenches were observed under TEM. Two main types of secondary particles, namely P1 and P2, were identified according to their compositions analysed by EDX, as shown in Fig. 2. In particular, P1 particles, containing Fe, Si and Mn, were observed in all samples, while P2 particles which contain Mg and Si can be observed only in VC and AC conditions. P1 particles are mostly spherical or ellipsoidal, whereas P2 particles are mostly rod-shaped. P2 particles are found mainly growing on the P1 particles aligning along 〈100〉 directions of the Al matrix, and some of them are also found at grain boundaries.

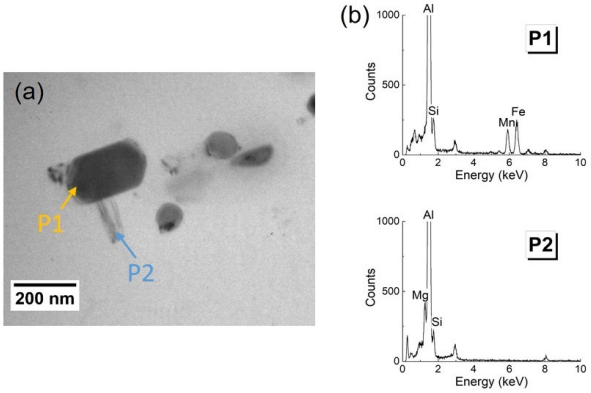

Fig. 2. (a) TEM micrograph of AC sample. (b) EDX analyses of the two particles in (a).

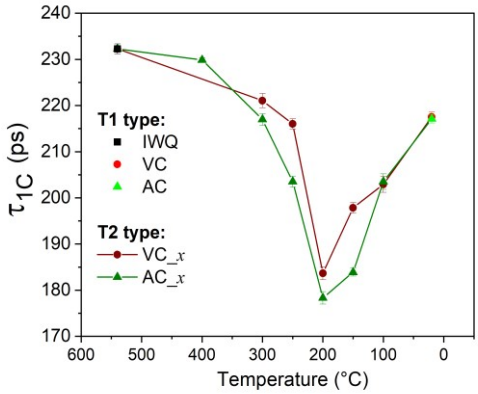

Fig. 3. One-component positron lifetimes after various T1 and T2 quenches.

3.2 Positron lifetime measurements

One component positron lifetimes τ_{1C} were measured after T1 and T2 type quenches (Fig. 3). After T1 type quenches, a positron lifetime of ~232 ps is obtained in IWQ sample, and ~217 ps is obtained in both VC and AC samples. Assuming the positron lifetime change during the fast quenching in ice water is negligible, the curves in Fig. 3 represent the lifetime evolution during VC and AC quenching. It is seen that during both quench routes, τ_{1C} first decrease and then increase. The

transition between the two stages is at 200 °C. The lowest lifetime is ~185 ps for VC_200 and ~179 ps for AC_200.

3.3 Hardness measurements

3.3.1 After direct artificial ageing

Hardening during AA of the alloy after SHT and various quench conditions is given in Fig. 4. For samples after T1-type quenches (complete quench to ambient temperature), the initial hardnesses are the same within ±1 HBW. The times needed to reach peak age are also similar for all conditions (4 h), while the peak hardnesses are lower for slower cooling, with 112 HBW, 108 HBW and 99 HBW for IWQ, VC, and AC, respectively. In contrast to the later stages, early stage hardening (i.e. up to 5 min) appears to be slightly stronger for the VC and AC samples than for IWQ. Two T2-type quenched conditions are subjected to AA, namely VC_200 and AC_200. They show slightly lower hardnesses (max. 2 HBW) than VC and AC samples in the as-quenched condition, but identical hardnesses after PB, and at peak age condition.

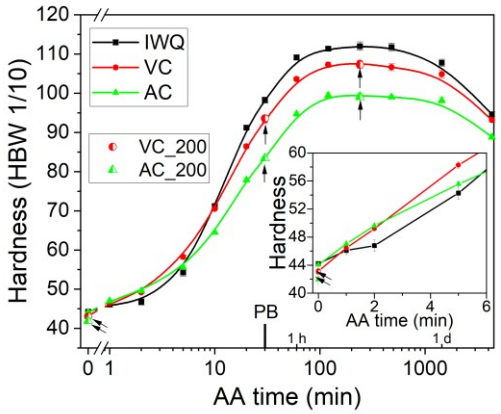

Fig. 4. Hardness of the alloy during AA after various T1 quenches and two T2 quenches. Inserted graph shows early stage AA on a linear time scale. Arrows denote the T2-type quenched samples.

3.3.2 After natural ageing and paint-baking

When nominally no NA is applied, PB leads to hardnesses of ~98 HBW, ~93 HBW, and ~83 HBW for IWQ, VC, and AC, respectively. As NA time increases, PB hardness initially declines rapidly and then levels off to a similar level (Fig. 5a). The absolute decrease of PB hardness after NA relative to the initial value is smaller for the slower cooled samples. Fig. 5b shows the relative PB decrease as a function of hardness increase during NA [12]. The influence of NA on PB hardening can be divided into two stages. During the first, the PB hardness decrease is significant and approximately proportional to the NA hardness increase. During the second, PB hardness decreases much slower and eventually stagnates although NA still hardens the material. The transition between the stages occurs at different NA hardnesses, whereas the corresponding NA times are quite similar for all quenched conditions, namely 90 min or 120 min.

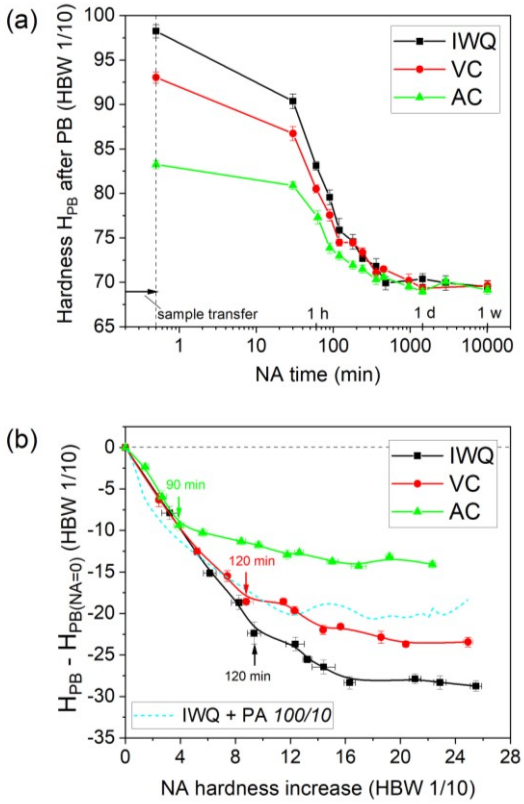

Fig. 5. (a) PB hardness after various NA times. First points are after NA for ~0.5 min, the interval for transferring samples from the cooling device to the oil bath for ageing. (b) Decrease of PB hardness plotted as a function of the hardness increase after NA (from Ref. [12]). NA time is an implicit parameter in both (b). The blue dashed curve in (b) is the corresponding curve of an ice-water quenched sample pre-aged at 100 °C for 10 min and then NSA taken from our previous study [9].

3.3.3 After pre-ageing, natural secondary ageing, and/or paint-baking

Applying PA effectively suppresses hardening during subsequent NSA, the extent of which depends on PA temperature and time (Fig. 6a) but hardly on whether IWQ or VC has been employed (the small offset ±1 HBW might reflect effects of different alloy batches). Longer PA at 100 °C (from 10 min to 4 h) causes a stronger suppression on NSA. When similar PA hardness is achieved by PA at 100 °C for 4 h and 140 °C for 30 min, NSA hardening kinetics for PA conducted at 100 °C is slower.

IWQ and VC samples behave differently when a final PB treatment is performed after PA (Fig. 6b, 1st, 3rd and 5th columns). For the same ageing condition, VC samples age to a lower PB hardness than IWQ samples. These hardness differences are reduced when 4 weeks of NSA are introduced after PA (2nd and 4th columns). When comparing PA treatments at different temperatures that lead to similar hardness, PA at 140 °C appears to be superior for achieving a higher PB

hardness for both IWQ and VC samples (3rd vs. 5th column). Therefore, the finding previously found for IWQ samples [9] is still applicable to slower cooled samples, i.e. at lower PA temperature the alloy shows slower NSA hardening while at higher PA temperature a higher PB potential is encountered

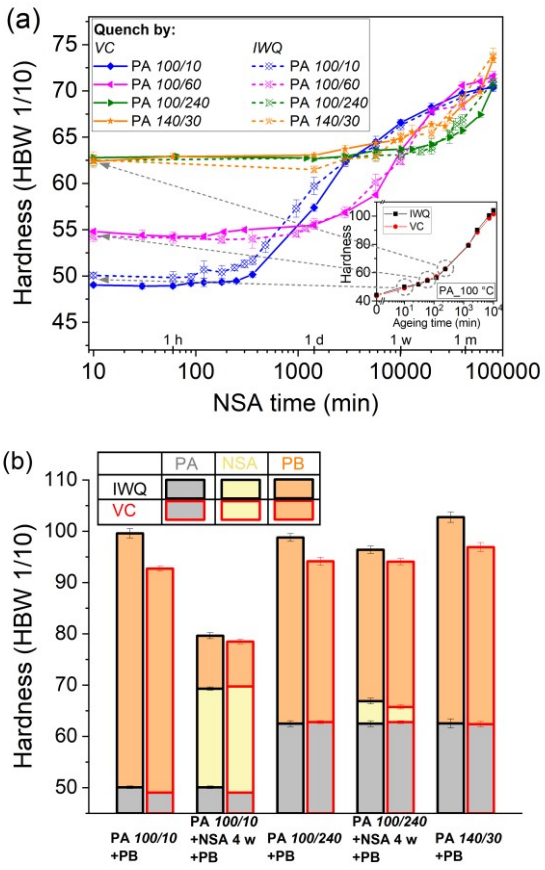

Fig. 6. Comparison of the hardness of IWQ and VC samples (a) during NSA after various PA treatments, and (b) after PB of various aged states. Inserted graph in (a) shows hardness during PA at 100 °C up to 1 week. Data for IWQ taken from Ref. [9].

4 Discussion

4.1 Influence of quenching conditions on as-quenched states

The microstructure after quenching is markedly influenced by the quench rate as primarily reflected by the TEM and PALS results. Fe-containing particles (P1 in Fig. 2a) found in all samples are dispersoids typically formed during homogenization [13, 14], whereas the Mg-Si containing particles (P2) are only found in VC and AC samples but not for IWQ, indicating that they are precipitates formed during quenching. Fast quenching in IWQ suppresses the formation of such precipitates. By measuring the in-situ heat evolution during cooling, Milkereit et al. characterised two precipitation reactions [1, 2]: A high-temperature reaction occurring typically from 500 °C down to ~380 °C represents the precipitation of equilibrium β phase, while a low-temperature reaction happens from 380 °C down to ~250 °C and stands for precipitation of β' and B′ phases. The high-temperature reaction is negligible for quench rates higher than 0.17 K/s [1]. Similar results were obtained by Strobel et al. [11]. This and the observation that the shape of the precipitates we find is closer to β' and B′ as described in Ref. [1] instead of to the typical plate shape for β imply that for our quenching conditions, the low-temperature reaction is dominant. As precipitates are mostly attached to dispersoids these seem to be their nucleation sites in accordance with the literature [15-18].

One component positron lifetime τ_{1C} represents a weighted average of positron lifetimes in various microstructural features, most importantly in mono-vacancies (~245 ps), solute clusters (~210 to 220 ps), and bulk Al (≤160 ps) [19]. After fast quenching (IWQ), the high lifetime (~232 ps) indicates a very high vacancy concentration so that positrons are annihilated mostly in vacancies. During slow quenching (VC and AC) down to 200 °C, lifetime decreases to a level close to 160 ps. This can only be caused by a substantial reduction of vacancies due to their high mobility at high temperature and consequently annihilating at vacancy sinks under the thermodynamic driving force. A rough estimation shows the vacancy concentration after VC and AC are at least 1 – 2 orders of magnitude lower than after IWQ [12]. Further cooling to room temperature increases τ_{1C} to 217 ps, which should be due to clustering or nucleation of precipitates at this temperature regime. Fig. 4 shows that the clustering contribution to hardness increase during cooling is at the most 2 HBW (AC_200 compared with AC) or even unnoticeable (VC_200 compared with VC). This shows that positron lifetime is much more sensitive to the formation of very small clusters than hardness, possibly because initial small clusters can trap positrons but contribute little to hardness.

In summary, slower quenching reduces the vacancy site fraction markedly, lowers the solute supersaturation owing to pre-precipitation, and prompts solute clustering primarily below 200 °C.

4.2 Influence of quenching conditions on subsequent ageing

4.2.1 Artificial ageing hardening

Slower quenching leads to a higher loss of (i) dissolved solutes and (ii) vacancies, both negatively affecting the formation of precipitates during AA. (iii) The properties of the clusters formed during quenching could also differ and affect AA, depending on the type of clusters. It has been assumed that in solute-rich Al-Mg-Si alloys, clusters formed at PA temperature will act as nuclei of strengthening precipitates (mainly β'') during AA, whereas the clusters formed at NA temperature will cause a detrimental effect on AA [20]. From the PALS measurements (Fig. 3), clustering phenomena during cooling are observed mainly below 200 °C. Thus, AA after VC_200 (and AC_200) is an interesting reference state as only little prior precipitation has taken place

between 200 °C and 20 °C. The PB hardness as well as the peak-ageing hardness of VC_200 (and AC_200) treated samples are similar to those of the VC (and AC) samples in which clustering has taken place (Fig. 2). Cluster formation during quenching has therefore little negative impact on subsequent AA, which also implies that these clusters are primarily PA clusters that can develop into β'', most likely because most of them are formed notably above 'room temperature' during cooling.

Next, the influence of the three factors mentioned above on AA kinetics is discussed. The AA process is divided into various stages as schematically represented in Fig. 7 according to the evolution of hardness after two quenches, namely IWQ and VC. A possible scenario of the evolution of solute supersaturation (SS) and vacancy site fraction (VF) is deduced qualitatively. In the early stage AA (I in Fig. 7), a slightly higher hardening is observed for VC samples than for IWQ samples. As discussed above, SS and VF are both lower for VC sample than for the IWQ sample after quenching, and both factors should negatively influence the hardening rate. Therefore, it must be the clusters formed during VC that enhanced the precipitate formation during AA by acting as nuclei or precursors.

As ageing proceeds, the importance of these quenched-in clusters vanishes because more nuclei are gradually formed during AA. After that – in late stage I or early stage II – the hardening rate is dominated by the available solutes and vacancies. Thus, the hardness of IWQ samples increases faster and eventually exceeds the hardness of VC samples, until the largest difference is reached after ~30 min of AA (end of stage II). Subsequent ageing further hardens the material to the peak-ageing state, during which the difference between the two hardening curves remains approximately constant (stage III). This indicates that the SS and VF in two samples are very similar in this stage. In other words, the extra solute supersaturation in the IWQ sample has been fully transformed to the higher hardness at the latest by the end of stage II. However, the question remains which role the higher vacancy site fraction in IWQ than in VC during stage I and II plays. During AA at 180 °C, the vacancy concentration after quenching will move from highly excess towards the much lower thermal equilibrium. The positive influence on hardening kinetics of the high fraction of excess vacancies quenched-in by IWQ exists only until thermal equilibrium has been reached. If the equilibrium is reached rapidly in the early stage of AA (denoted as route '1' in Fig. 7) as predicted by simulations [21, 22], then the faster hardening in stage II for IWQ would be primarily due to the higher SS. However, if vacancy annihilation is not that fast (route '2' in Fig. 7), e.g. delayed by vacancy trapping in clusters, and a considerably higher vacancy concentration still continues to exist in IWQ samples than in VC samples for a few tens of minutes, then the higher hardening in stage II for IWQ would be caused by both higher SS and VF resulting from faster quenching. Which scenario is more likely cannot be deduced from the current measurements and remains to be further explored.

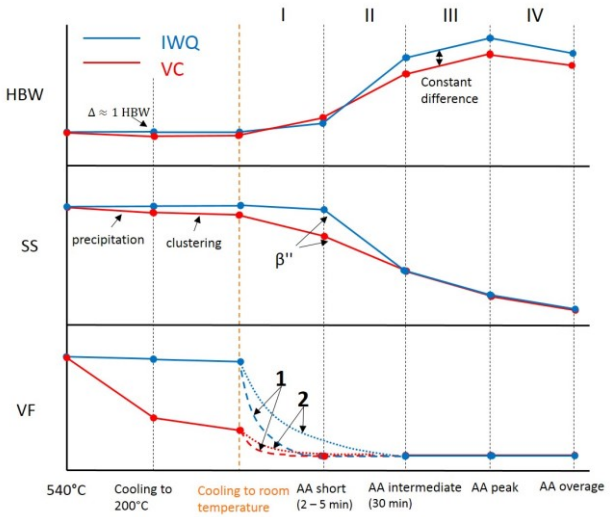

Fig. 7. Schematic graph of the evolution of hardness (HBW), solute supersaturation (SS), and vacancy site fraction (VF) during AA. '1' and '2' label the two possible vacancy evolution routes. This graph is meant to visualise the discussion and the lower two panels are not based on quantitative data.

4.2.2 Paint-baking hardening after natural ageing

The term 'negative effect' refers to the delayed AA hardening kinetics after NA and, more importantly in practice, the compromised PB hardness. The origin of the effect is widely attributed to the formation of NA clusters, although the exact mechanism is still in controversy. Serizawa et al. [20] and Aruga et al. [23] argue that the NA clusters are difficult to either grow into β'' or dissolve during AA, thus decreasing the supersaturation of solutes and consequently hardening during AA. Zandbergen et al. [24, 25] argue that the increase of the nucleation barrier for the β'' phase due to a decreased solute concentration after NA (even if only a few %) markedly suppresses nucleation of the β'' phase. Pogatscher et al. [26] attribute the retardation of AA hardening to the depletion of mobile excess vacancies which are "imprisoned" by the clusters formed during NA. To discuss which mechanism is more likely is out of the scope of the current study, but these quoted ideas allow us to discuss the distinct negative effects (Fig. 5 & Fig. 6b) introduced by different quench rates, i.e. why PB hardnesses are more similar after longer NA.

Fig. 5b now shows that the loss of PB hardness with progressing NA is not uniform but can be roughly divided into two stages and where the decrease mainly comes from the first stage. A similar slope for all the curves in this stage implies that the negative effect in differently quenched samples share some similarities. Each NA hardening by 1 HBW reduced PB hardness by ~2.3 HBW. The times for the first stage are all within the initial 120 min, pointing at initial NA cluster formation having the biggest effect on PB hardening. Such clusters are formed more in fast quenched sample than in slow quenched sample as the hardness at the end of first stage is increasing with higher quench rate and consequently

the decrease of PB hardness is larger too. The effects of these clusters can be two-fold. First, they lock solutes which will be temporarily not available for further precipitation. Second, they influence the mobile vacancy concentrations by trapping as described above. When there are few mobile vacancies available, the precipitation rate will be limited by the number of these vacancies which transport the solutes to precipitates. Thus, after long NA clustering, PB does not result in any hardening regardless of quench condition.

The formation of PA clusters during slow quenching could be another reason. PA is well known to suppress NA clustering and the negative effect. The corresponding decrease of PB hardness against the NSA hardening of a typical PA treatment after IWQ (PA at 100 °C for 10 min) from our previous study [9] is shown in Fig. 4b. Similar to slow quenching, PA also shows a reduced negative effect despite of the same hardness increase due to NA/NSA clustering. It has been discussed (Sec. 4.2.1) that these clusters are more important for the early stage AA when hardening is low. As hardness increases, the advantage of having these nuclei for slower quenched samples diminishes as a high amount of precipitates are formed also in the IWQ sample. Therefore, as PB response decreases due to progressing NA clustering, the importance of quenched-in PA clusters increases, which results in a smaller PB hardness loss.

4.2.3 Multi-stage ageing

Comparison of multi-stage ageing hardness after IWQ and VC suggests the PA and NSA hardening are almost independent of quenching conditions. Since vacancies are important for the NA clustering, it needs to be explained why the large vacancy difference after IWQ and VC influences little to NSA hardening. This might be due to two reasons: 1) the difference of NA clustering kinetics after various quenching conditions is much smaller than expected, possibly associated to vacancy clustering or strong vacancy trapping at early stage of NA [12]; 2) the vacancy difference is narrowed after PA as distinct vacancy concentrations are moving towards the same equilibrium concentration during the process. Consequently, the NSA clustering depends less on quench rate but more on the PA condition, the effect of which depends primarily on PA temperature [9]. Final PB is lower for slower-quenched samples as PB is more dependent on solute supersaturation, which is lower in those samples.

5 Conclusions

We have investigated the influence of quenching conditions (quench rate: IWQ>VC>AC) after SHT on the microstructure and subsequent multi-stage age-hardening kinetics of an AA6014 alloy by means of TEM, hardness, and PALS measurements. We find:

- During slow quenching (VC or AC), precipitates are formed primarily on dispersoids and at grain boundaries unlike in the fast quenched IWQ sample. More vacancies annihilate during quenching before reaching 200 °C for slower quenching, as observed by positron lifetime measurements. Clusters are primarily formed during quenching below 200 °C.
- The AA hardness for slower quenched samples is initially slightly higher compared to faster quenched samples due to the formation of PA clusters or nuclei for precipitates during quenching, but later in technologically more important later stages of AA falls back due to a lower solute supersaturation.
- PB hardening is higher for faster quenched samples when no NA or no NSA is applied. However, the influence of quenching rate gradually diminishes as NA or NSA becomes longer. Less formation of clusters in the initial NA stage and the formation of PA clusters during quenching may contribute to this effect.
- Multi-stage age hardening for samples after IWQ and VC (simulated industrial quench) are similar, with almost identical PA+NSA hardening and only slightly lower PB hardening for VC samples. The trade-off effect previously found for samples after IWQ still applies for VC conditions, i.e., PA at lower temperature enhances the stability during subsequent NSA but decreases the maximum PB hardening potential and vice versa.

The industry can benefit from this study as most of the findings in laboratory regarding the study of multi-stage ageing can be now directly applied to the industrial conditions, only to consider a slightly higher PB hardening loss in industrial practice.

Acknowledgements

The authors would like to thank Mrs. Christiane Förster for TEM sample preparation and Dr. Anna Manzoni for her help with the TEM measurements.

References

1. B. Milkereit, N. Wanderka, C. Schick and O. Kessler, Materials Science and Engineering A **550**, 87-96 (2012)
2. B. Milkereit and M. J. Starink, Materials & Design **76**, 117-129 (2015)
3. J. L. Cavazos and R. Colas, Materials Science and Engineering A **363**, 171-178 (2003)
4. P. Brenner and H. Kostron, Zeitschrift für Metallkunde **31**, 89-97 (1939)
5. D. W. Pashley, J. W. Rhodes and A. Sendorek, Journal of the Institute of Metals London **94**, 41-49 (1966)
6. M. Saga, Y. Sasaki, M. Kikuchi, Z. Yan and M. Matsuo, Materials Science Forum **217**, 821-826 (1996)
7. L. Zhen and S. B. Kang, Scripta Materialia **36**, 1089-1094 (1997)
8. Y. Takaki, Y. Aruga, M. Kozuka and T. Sato, Materials Science Forum **794-796**, 1026-1031 (2014)

9. Z. Yang, Z. Liang, D. Leyvraz and J. Banhart, Materialia **7**, 100413 (2019)
10. K. Strobel, M. D. H. Lay, M. A. Easton, L. Sweet, S. Zhu, N. C. Parson and A. J. Hill, Materials Characterization **111**, 43-52 (2016)
11. K. Strobel, M. A. Easton, M. D. H. Lay, P. A. Rometsch, S. Zhu, L. Sweet, N. C. Parson and A. J. Hill, Metallurgical and Materials Transaction A **50A**, 1957-1969 (2019)
12. Z. Yang, X. Jiang, X. Zhang, M. Liu, Z. Liang, D. Leyvraz and J. Banhart, Scripta Materialia (accepted for publishing)
13. H. Hirasawa, Scripta Metallurgica **9**, 955-958 (1975)
14. L. Lodgaard and N. Ryum, Materials Science and Engineering A **283**, 144-152 (2000)
15. A. Dons and O. Lohne, MRS Proceedings **21**, 723-728 (1983)
16. S. Zajac, B. Bengtsson and C. Jönsson, Materials Science Forum **396-402**, 399-404 (2002)
17. K. Strobel, M. A. Easton, L. Sweet, M. J. Couper and J. F. Nie, Materials Transactions **52**, 914-919 (2011)
18. P. A. Rometsch, S. C. Wang, A. Harriss, P. J. Gregson and M. J. Starink, Materials Science Forum **396-4**, 655-660 (2002)
19. M. Liu, J. Cizek, C. S. T. Chang and J. Banhart, Acta Materialia **91**, 355–364 (2015)
20. A. Serizawa, S. Hirosawa and T. Sato, Metallurgical and Materials Transactions A **39A**, 245-251 (2008)
21. S. Pogatscher, E. Kozeschnik, H. Antrekowitsch, M. Werinos, S. S. A. Gerstl, J. F. Loffler and P. J. Uggowitzer, Scripta Materialia **89**, 53-56 (2014)
22. A. Falahati, P. Lang and E. Kozeschnik, Materials Science Forum **706-709**, 317-322 (2012)
23. Y. Aruga, M. Kozuka, Y. Takaki and T. Sato, Materials Science and Engineering: A **631**, 86-96 (2015)
24. M. W. Zandbergen, Q. Xu, A. Cerezo and G. D. W. Smith, Acta Materialia **101**, 136-148 (2015)
25. M. W. Zandbergen, Q. Xu, A. Cerezo and G. D. W. Smith, Data in Brief **5**, 626-641 (2015)
26. S. Pogatscher, H. Antrekowitsch, H. Leitner, T. Ebner and P. J. Uggowitzer, Acta Materialia **59**, 3352-3363 (2011)